SPACE WEATHER, VOL. 4, S08001, doi:10.1029/2005SW000204, 2006

Real-time cosmic ray monitoring system for space weather

T. Kuwabara,[1] J. W. Bieber,[1] J. Clem,[1] P. Evenson,[1] R. Pyle,[1] K. Munakata,[2] S. Yasue,[2] C. Kato,[2] S. Akahane,[2] M. Koyama,[2] Z. Fujii,[3] M. L. Duldig,[4] J. E. Humble,[5] M. R. Silva,[6] N. B. Trivedi,[6] W. D. Gonzalez,[6] and N. J. Schuch[6]

Received 29 October 2005; revised 25 January 2006; accepted 26 January 2006; published 15 August 2006.

[1] We have developed a real-time system to monitor high-energy cosmic rays for use in space weather forecasting and specification. Neutron monitors and muon detectors are used for our system, making it possible to observe cosmic rays with dual energy range observations. In large solar energetic particle (SEP) events, the ground level enhancement (GLE) can provide the earliest alert for the onset of the SEP event. The loss cone precursor anisotropy predicts the arrival of interplanetary shocks and the associated interplanetary coronal mass ejections (ICMEs), while the occurrence of bidirectional cosmic ray streaming indicates that Earth is within a large ICME. This article describes a set of real-time Web displays that clearly show the appearance of the GLE, loss cone precursor, and other space weather phenomena related to cosmic rays.

Citation: Kuwabara, T., et al. (2006), Real-time cosmic ray monitoring system for space weather, *Space Weather*, *4*, S08001, doi:10.1029/2005SW000204.

1. Introduction

[2] Owing to the large detector mass required to detect high-energy cosmic rays, ground-based instruments remain the state-of-the-art method for studying these elusive particles [*Simpson et al.*, 1953; *McDonald*, 2000]. Neutron monitors and muon detectors record secondary cosmic rays created by interactions of >1 GeV primary cosmic rays (predominantly protons and heavier nuclei) with Earth's atmosphere. These cosmic rays are the dominant source of ionization in Earth's upper atmosphere and are a major source of natural radiation on Earth's surface. In addition, at energies up to ~100 GeV, primary galactic cosmic rays experience significant variation in response to passing solar wind disturbances such as interplanetary coronal mass ejections (ICMEs). With suitable analysis, ground-based detectors can yield unique information on conditions in the near-Earth interplanetary medium.

[3] Neutron monitors can also detect the most energetic solar energetic particle (SEP) events. SEPs that propagate to Earth can cause damage to satellite electronics and can pose a radiation hazard to astronauts and air crews. In the typical SEP event, the particle flux increases in the 10–100 MeV energy range, but these energies are insufficient to produce an effect in ground level detectors. However, in the most extreme SEP events, the particle flux increases at energies >500 MeV, and these can be detected by ground-based neutron monitors as a ground level enhancement (GLE). A sample SEP event analyzed by *Bieber et al.* [2004] is shown in Figure 1. Because the propagation speed of SEPs along the interplanetary magnetic field (IMF) depends upon energy, the start time of the intensity increase in the neutron monitors (bottom plot) is earlier than that of the low-energy proton flux (top plot). Furthermore, time to reach maximum intensity is also shorter at higher energy. Consequently, GLE observations make it possible to warn of the arrival of the SEP event earlier than methods based upon lower-energy charged particles.

[4] ICMEs and their accompanying shocks, if present, reach Earth within a few days and may cause a geomagnetic storm. Because geomagnetic (and ionospheric) storms can affect society by disrupting radio communications, GPS navigation, and electronic power systems on the ground, it is important to detect oncoming ICMEs. CMEs can be detected near the Sun by optical measurements aboard satellites. But near Earth, in situ satellite observations at the L1 point give only ~1 hour advance warning of the arrival of shocks and ICMEs. When a shock

[1]Bartol Research Institute and Department of Physics and Astronomy, University of Delaware, Newark, Delaware, USA.
[2]Physics Department, Shinshu University, Matsumoto, Japan.
[3]Solar-Terrestrial Environment Laboratory, Nagoya University, Nagoya, Japan.
[4]Australian Antarctic Division, Kingston, Tasmania, Australia.
[5]School of Mathematics and Physics, University of Tasmania, Hobart, Tasmania, Australia.
[6]National Institute for Space Research, Sao Jose dos Campos, Santa Maria, Brazil.

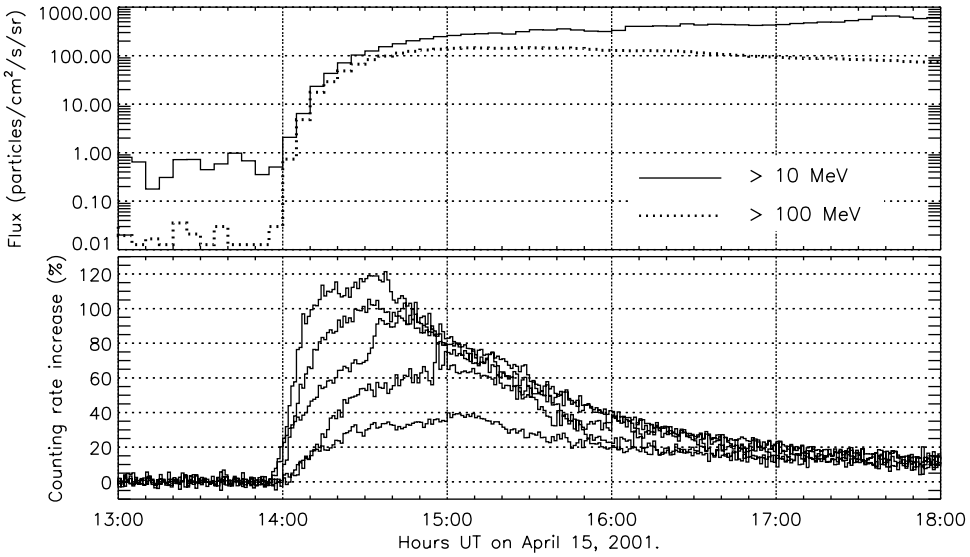

Figure 1. SEP event on 15 April 2001: (top) low-energy proton integral flux at GOES 10 satellite (solid line, >10 MeV; dotted line, >100 MeV) and (bottom) neutron rates detected in several neutron monitors. Plotted are 5-min and 1-min average values for proton and neutron data, respectively. Note that the neutron monitor onset clearly preceded the GOES onset.

approaches Earth, sometimes we can see a loss cone precursor, that is, a strong suppression of cosmic ray intensity for particles arriving from the sunward magnetic field direction. Loss cone precursors have generally been interpreted as kinetic effects related to interaction of ambient galactic cosmic rays with the approaching shock [*Nagashima et al.*, 1994; *Belov et al.*, 1995; *Morishita et al.*, 1997; *Ruffolo*, 1999; *Leerungnavarat et al.*, 2003]. Typical lead times of the loss cone precursor are 4 hours for neutron monitors [*Belov et al.*, 2001]. For muon detectors, lead times are typically 8 hours and more than 24 hours in rare cases [*Munakata et al.*, 2000]. Thus it is possible to use this phenomenon as a warning of a geomagnetic storm.

[5] Some other information about the ICME is also seen in the cosmic ray intensity variation after the shock passage. Cosmic ray intensity decrease, called Forbush decrease [*Forbush*, 1938], is caused by passage of the cosmic ray density-depleted region formed behind the shock and inside the ICME (ejecta). From this phenomenon we can identify whether and when the ICME passes Earth [*Cane*, 2000], and we can determine how big it is. Within and around the cosmic ray–depleted region, there may be a $\mathbf{B} \times \nabla n$ drift flow driven by a density gradient perpendicular to the IMF [*Bieber and Evenson*, 1998]. Since this drift flow sometimes appears before the shock passage [*Munakata et al.*, 2005], it can be useful for space weather forecasting. Cosmic rays within a large ICME often display field-aligned "bidirectional streaming" [*Dvornikov et al.*, 1983; *Dvornikov and Sdobnov*, 2002; *Richardson et al.*, 2000], in a manner similar to the bidirectional electrons observed at much lower energy [*Gosling et al.*, 1990]. This phenomenon provides us with information about when Earth is within a large ejecta region.

[6] To evaluate the usefulness of these various phenomena for space weather forecasting, it is necessary to consider their occurrence rates. In a recent study from ~5 years' neutron monitor data, we found that 11 GLEs observed in this period were all accompanied by solar radiation storms. Using solar radiation storm levels from the Space Environment Center of NOAA (NOAA Space Environment Center Web site, http://www.sec.noaa.gov), the occurrence rate of GLEs was 29% for S2 or greater storms, 36% for S3 or greater storms, and 40% for S4 storms. Details will be provided in a forthcoming publication.

[7] *Belov et al.* [2001] studied the occurrence rate of precursors in neutron monitor data prior to the 14 "major" ($Kp \geq 8-$) geomagnetic storms tabulated by *Gosling et al.* [1990] over the period 1978--1982. Precursors were detected in 11 of 14 storms (79%). Of these, seven were loss cone precursors (50% overall), and the remainder (four) were of a different type termed "enhanced variance" precursors. For muon detectors, the occurrence rate of precursors was calculated by *Munakata et al.* [2000] from 39 storms that include the 14 major storms of *Gosling et al.* [1990], supplemented by 25 "large" ($Kp \geq 7-$) storms over the period 1992–1998. After omitting 17 storms where the detectors had poor coverage of the pitch angle distribution, precursors were detected in 15 of the remaining 22 storms (68%), including 10 (45% overall) of the loss cone type and 5 of the enhanced variance type.

[8] Again, using the *Gosling et al.* [1990] list of major geomagnetic storms, *Bieber et al.* [1999] looked for evidence

Table 1. Information on the 15 Neutron Monitors Used in This Work[a]

Station	Type	Longitude	Latitude	Altitude, m
		Spaceship Earth Network		
Inuvik, Canada	18NM64	68.4 N	133.7 W	68
Fort Smith, Canada	18NM64	60.0 N	111.9 W	203
Peawanuck, Canada	18NM64	55.0 N	85.4 W	52
Nain, Canada	18NM64	56.5 N	61.7 W	46
Mawson, Antarctica	18NM64	67.6 S	62.9 E	30
Apatity, Russia	18NM64	67.6 N	33.4 E	181
Norilsk, Russia	18NM64	69.3 N	88.1 E	0
Tixie Bay, Russia	18NM64	71.4 N	128.5 E	0
Cape Schmidt, Russia	12NM64	68.6 N	180.3 E	0
Thule, Greenland	18NM64	76.5 N	68.7 W	26
McMurdo, Antarctica	18NM64	77.9 S	166.6 E	48
		Other Monitors		
South Pole, Antarctica	3NM64	90.0 S	0.0 E	2820
South Pole Bares	6NM64	90.0 S	0.0 E	2820
Barentsburg, Norway	6NM64	78.1 N	14.2 E	54
Newark, USA	9NM64	39.7 N	75.7 W	50

[a]Station name, detector type, geographical longitude, latitude, and altitude are listed for each station. Neutron monitors belonging to the Spaceship Earth network appear in the top rows. In the bottom rows, South Pole is a standard 3NM64, while South Pole Bares is our ''polar bare,'' a 6NM64 without the usual lead shielding. It responds to a slightly lower energy primary cosmic ray than the standard monitor.

of bidirectional cosmic ray streaming within the ejecta associated with these storms. Bidirectional streaming was clearly detected in neutron monitor data in 10 of the 14 events (71%). Thus bidirectional cosmic ray streaming appears to be a common phenomenon at neutron monitor energies, at least for the largest storms.

[9] We stress that the studies cited above were retrospective, and the success rates reported in them may well be higher than is attainable with the present real-time network. In particular, the retrospective studies of neutron monitor data generally used more stations than are currently available in real time. We expect the performance of real-time cosmic ray networks to steadily improve as more stations are brought online in real time.

[10] In the remainder of this article, we describe our real-time monitoring system of cosmic rays. Section 2 provides information on our detectors. Section 3 provides the details of our monitoring system, including some discussion of analysis methods.

2. Cosmic Ray Observations

[11] We have been developing methods for making real-time observations of the cosmic ray intensity and anisotropy using networks of neutron monitors and muon detectors. Since GLE and loss cone precursors are inherently anisotropic intensity variations, it is necessary to make a detector network providing continuous coverage of the complete range of pitch angles.

[12] Neutron monitors and muon detectors record the by-products of nuclear interactions of high-energy primary cosmic rays with Earth's atmosphere. Because the primary energies that neutron monitors detect are comparatively low ($\sim$2 GeV for solar particles and $\sim$17 GeV for galactic cosmic rays), while those that muon detectors detect are comparatively high ($\sim$50 GeV for galactic cosmic rays), the two instrument types provide complementary observations. For example, the neutron monitor is much more likely to detect an SEP event whereas the muon detector is expected to provide earlier detection of the loss cone precursor [*Leerungnavarat et al.*, 2003]. In addition, the energy dependence of many phenomena can be determined by the comparison of these networks' data.

2.1. Neutron Monitors

[13] In this work we use 15 neutron monitor stations that include 11 Spaceship Earth stations and four other stations. Information on all stations is presented in Table 1. Spaceship Earth stations, shown in the top 11 rows in Table 1, make a network of neutron monitors strategically located at high latitude to provide optimum directional sensitivity and three-dimensional measurements of the angular distribution of solar cosmic rays [*Bieber and Evenson*, 1995]. The viewing direction for primary protons is displayed in Figure 2. Squares show asymptotic viewing directions for a median energy particle, and the lines show the range of viewing directions for the central 80% of the detector energy response. All stations (solid circles) are at high geographic latitudes, but nine of them view the equatorial region after accounting for bending of particle trajectories in the geomagnetic field, while Thule and McMurdo generally view the Northern and Southern hemispheres, respectively. Assuming a nominal P^{-5} spectrum for solar cosmic rays, this network covers the primary rigidity range from 1.05 GV (at 10th-percentile rigidity) to 5.33 GV (at 90th-percentile rigidity). The median rigidity is 2.14 GV.

2.2. Muon Detectors

[14] For muon detectors, we use the three stations represented in Table 2. The muons are highly penetrating and

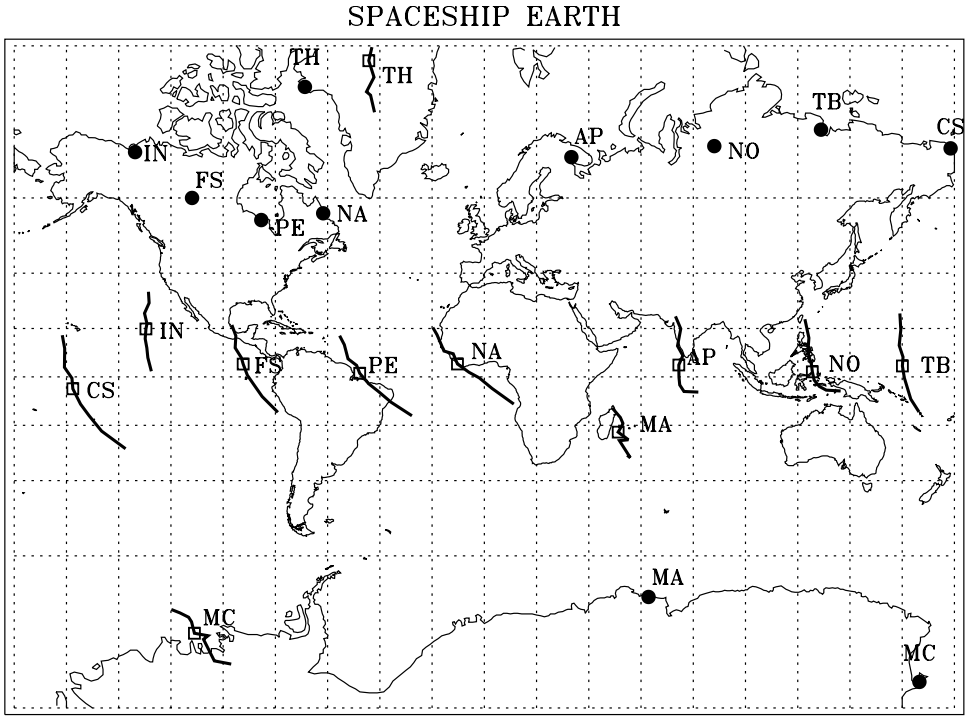

Figure 2. Viewing direction of the Spaceship Earth neutron monitor network for an assumed P^{-5} solar particle spectrum. Solid circles show station locations, squares show asymptotic viewing directions for a median energy particle, and lines show the range of viewing directions for the central 80% of the detector energy response. Two-letter station codes correspond to the first two letters of the station name or the first letter of each word in the case of a two-word name.

retain the directional information of the primary proton. For this reason, each detector has multiple directional channels and can cover a wide range of viewing directions over Earth. The viewing direction for primary protons is displayed in Figure 3. Each of the symbols shows asymptotic viewing directions for a median rigidity particle, assuming a galactic spectrum of primary cosmic rays, and the lines through the symbols show the range of viewing directions for the central 80% of the energy response. Because the energy response varies with the inclination of each directional channel, the median rigidity of primary cosmic rays recorded for the different directions ranges from 56 to 119 GV, while the 10th-percentile rigidity ranges from 16 to 38 GV, and the 90th-percentile rigidity ranges from 359 to 890 GV. The detection area of the São Martinho station was increased from 4 to 28 m^2 in December 2005, and the number of viewing directions was increased from 9 to 17. (Even more viewing directions are available from this instrument and may be incorporated into our analysis in the future.)

3. Data Display

[15] The following graphs are now available to show cosmic ray phenomena related to interplanetary disturbances: GLE monitor, cosmic ray pitch angle distribution (loss cone display and bidirectional streaming display), cosmic ray flow direction, and individual station count rates. These graphs are automatically made in real time and are updated on the following Web site: http://neutronm.bartol.udel.edu/spaceweather/.

Table 2. Information on Muon Detectors[a]

Station	Area, m^2	Direction	Latitude	Longitude	Altitude, m
Nagoya, Japan	36	17	35.2 N	137.0 E	17
Hobart, Australia	9	13	43.0 S	147.3 E	65
São Martinho, Brazil[b]	28	17	29.4 S	306.2 E	488

[a]Station name, detection area, number of viewing directions, geographical longitude and latitude, and altitude are listed for each station.
[b]São Martinho was upgraded from 4 to 28 m^2 and from 9 to 17 viewing directions in December 2005.

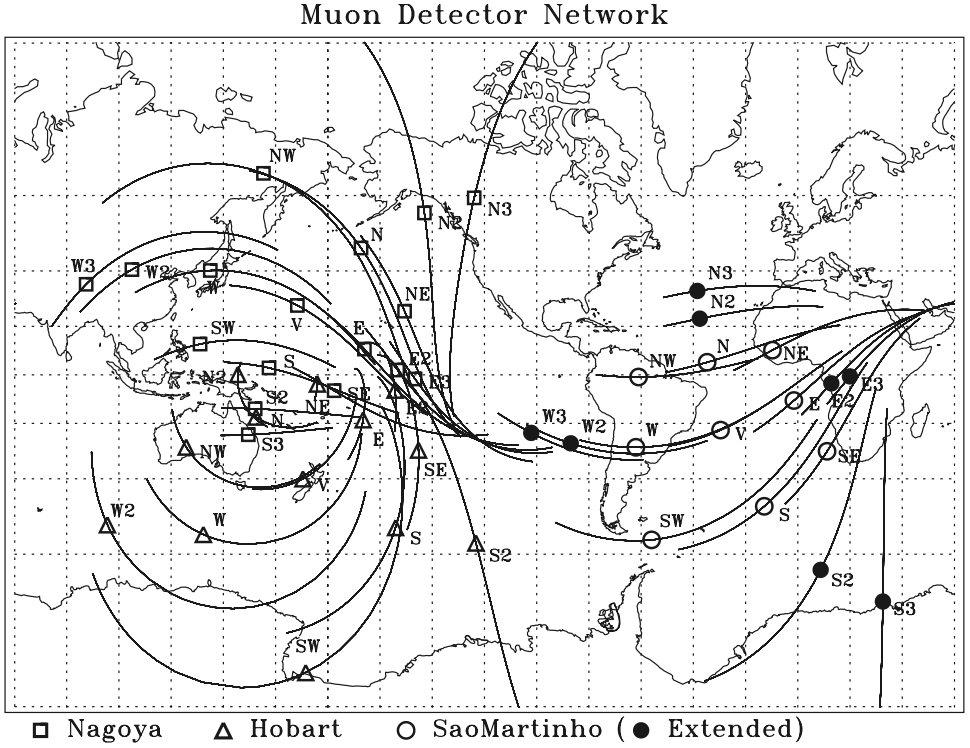

Figure 3. Viewing directions of the muon detector network. Each of the symbols (squares for Nagoya, triangles for Hobart, and circles for São Martinho) shows asymptotic viewing directions for a median rigidity particle, and the lines through the symbols show the range of viewing directions for the central 80% of the detector energy response. The number of viewing directions of the São Martinho detector was increased from 9 directions (open circles) to 17 directions (includes solid circles) in December 2005.

3.1. GLE Monitor

[16] The GLE monitor can be used as an early warning of a large SEP event. Since SEP events are only rarely detectable in the muon energy region, we display only neutron monitor data. A sample graph GLE monitor is displayed in Figure 4. Each line shows the pressure-corrected 1-min data from 11 Spaceship Earth stations and 3 other high-latitude stations. The 3 extra stations include South Pole, which, by virtue of its unique location at both high latitude and high altitude, is the world's most sensitive detector of high-energy solar cosmic rays.

[17] When a GLE occurs, a smooth rise at one or more stations (preferably more for confirmation) occurs over a period of 15 min or more and is followed by a (usually) slower decay. Generally, the GLE monitor will be of interest only during GLEs or major Forbush decreases. Most of the time, the displayed variations are simply statistical noise. Isolated spikes are probably data glitches and should be ignored if unconfirmed by other stations. We are currently developing an automated system to send out e-mail alerts when a GLE onset occurs. We are studying optimal strategies for detecting the event at a very early stage, while still keeping the false alarm rate at a very low level. Preliminary indications are that the GLE alert would precede the earliest alert from GOES (100 MeV or 10 MeV protons) by $\sim$10–30 min. Details will be provided in a forthcoming publication.

3.2. Loss Cone Display and Bidirectional Streaming Display

[18] The loss cone display can be used to warn of an approaching shock. The bidirectional streaming display can be used to indicate when Earth is within a large ICME. These phenomena are observed as a pitch angle anisotropy along the IMF, so it is necessary to display the pitch angle distribution of the intensity separately from the cosmic ray density (isotropic component). Furthermore, the bidirectional streaming is observed as higher-order anisotropy; hence it is best to display the residual anisotropy after subtracting both the density and the first-order anisotropy.

[19] The cosmic ray density and first-order anisotropy are deduced from a best fit calculation. Spaceship Earth pressure-corrected hourly count rates are internormalized to the McMurdo station by using a 24-hour trailing mov-

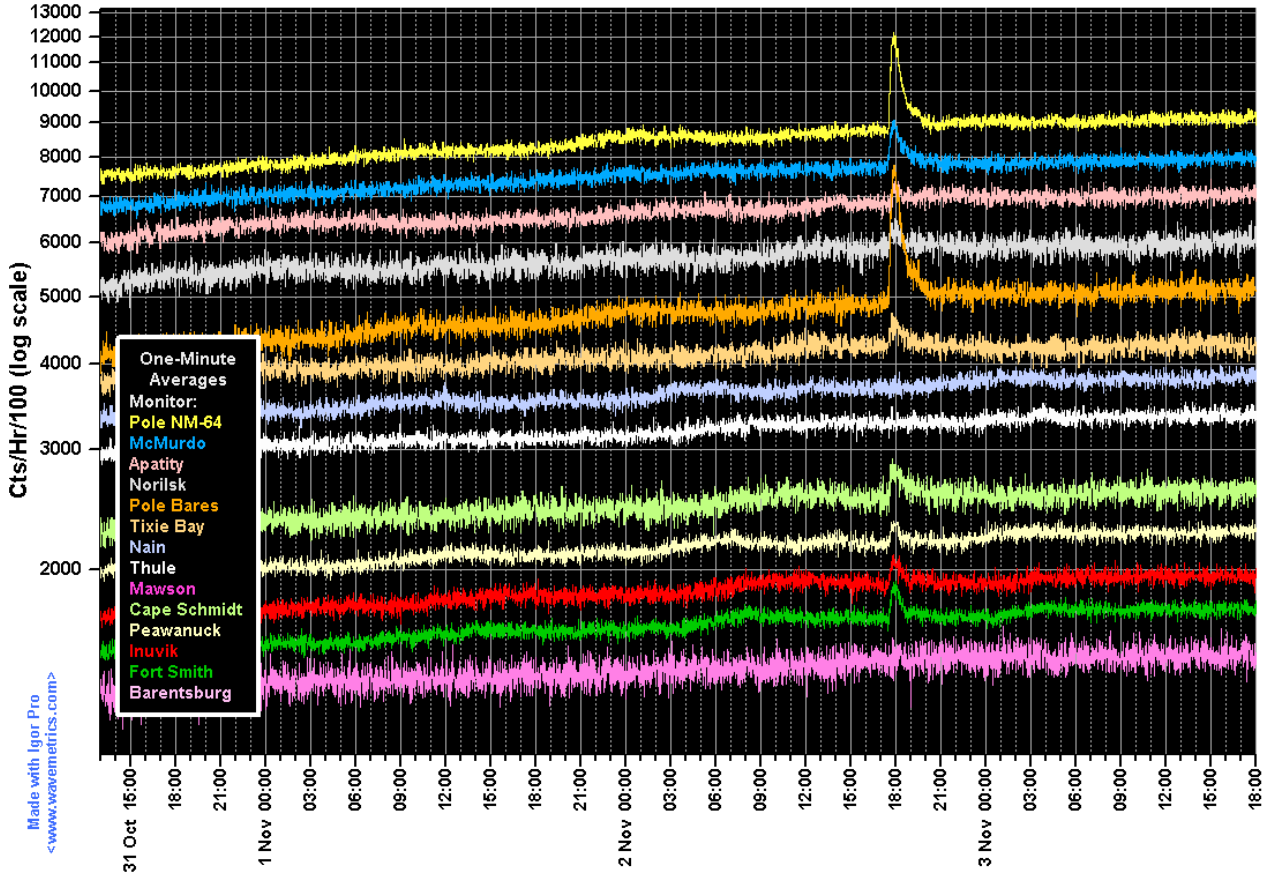

Figure 4. Sample GLE monitor in November 2003. Plotted are 1-min average counting rates detected by 14 stations during a period that a GLE was observed. (Unfortunately, Mawson was not operating during this period.) These include the 11 Spaceship Earth stations and 3 additional ones. Some station count rates are multiplied by a factor, which varied depending on the station, to avoid overlap of data.

ing average. For each hour, these count rates are then fitted to a function representing a first-order anisotropy,

$$f(\theta,\phi) = n\left(1 + \xi_x \sin\theta\cos\phi + \xi_y \sin\theta\sin\phi + \xi_z \cos\theta\right), \quad (1)$$

where $f(\theta, \phi)$ is the normalized count rate measured by a station with an asymptotic viewing direction defined by θ (colatitude) and ϕ (longitude), n is the particle density, and ξ_x, ξ_y, and ξ_z are the three components of the anisotropy vector in the geocentric solar ecliptic (GSE) coordinate system. Because the Spaceship Earth stations have excellent angular resolution (Figure 2), we choose to represent the station-viewing direction by a single direction in space. Currently, we use the direction corresponding to a 6.1 GV proton, which is intermediate between the median rigidity of a solar particle spectrum (~2 GV) and the median rigidity of a galactic spectrum (~17 GV), as calculated from the neutron monitor response function [*Clem and Dorman*, 2000]. The use of a value less than that of a galactic spectrum is motivated by the fact that the depths of Forbush decreases tend to scale inversely with rigidity [*Morishita et al.*, 1990].

[20] For muon detector data, we obtain the percent deviation of the pressure-corrected hourly count rate, and these data are internormalized to the Nagoya vertical direction using a 24-hour trailing moving average. Because of the wide asymptotic cone as shown in Figure 3, it is not sufficient to represent each viewing direction with a single direction in space. Then, to deduce the exact anisotropy in space, the best fit function is defined by using the "coupling coefficients" [*Fujimoto et al.*, 1984] which relate the observed muon intensity variation to the primary cosmic ray intensity variation in free space. The best fit function becomes

$$I_{i,j}^{fit}(t_i) = Ic_{0i,j}^{0} + \xi_x^{\mathrm{GEO}}\left(c_{1i,j}^{1}\cos\omega t_i - s_{1i,j}^{1}\sin\omega t_i\right) + \xi_y^{\mathrm{GEO}} \cdot \left(s_{1i,j}^{1}\cos\omega t_i + c_{1i,j}^{1}\sin\omega t_i\right) + \xi_z^{\mathrm{GEO}} c_{1i,j}^{0}, \quad (2)$$

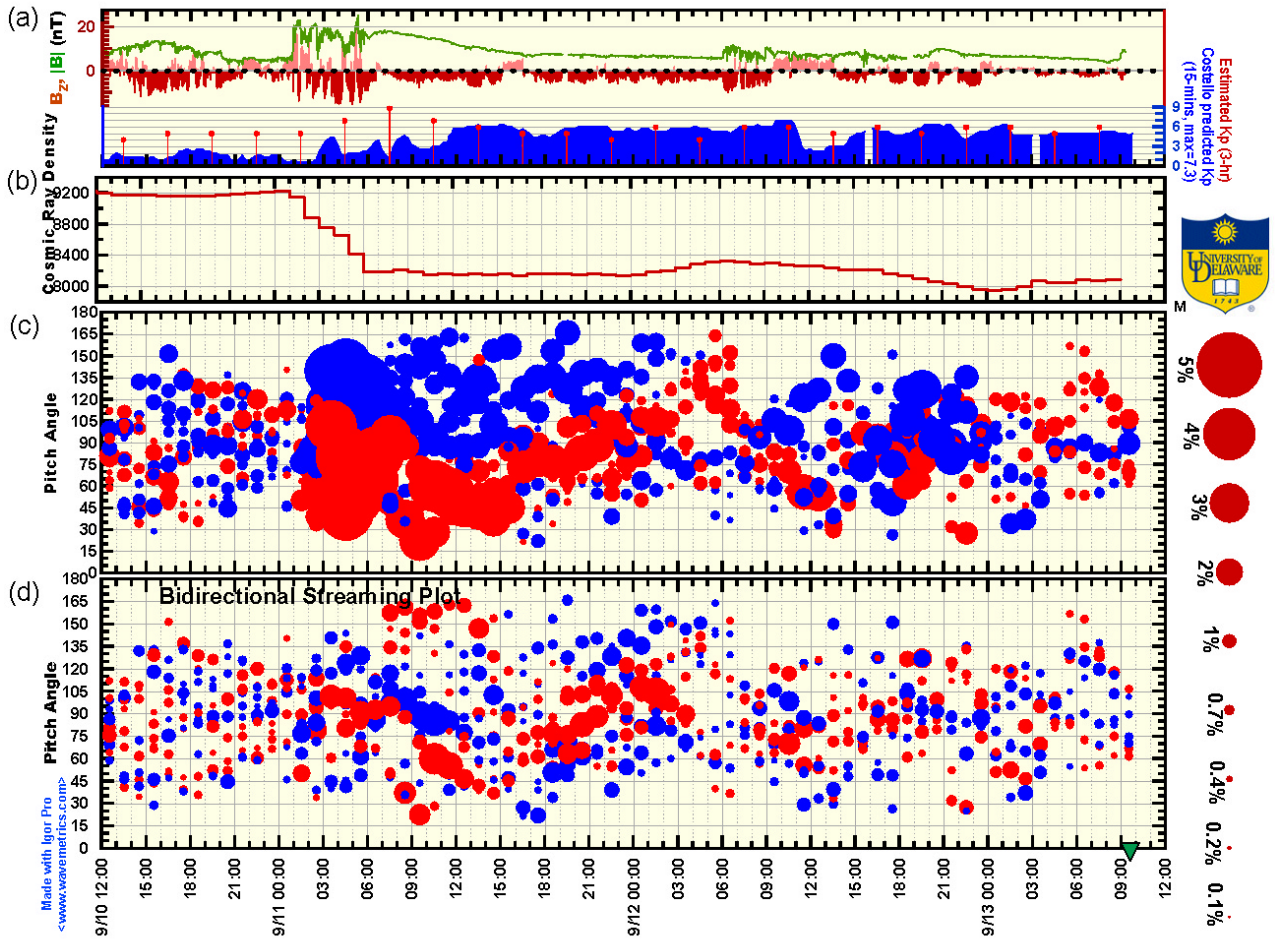

Figure 5. Sample loss cone display and bidirectional streaming display in September 2005. (a) Plotted are 1-min ACE magnetic field magnitude $|B|$ (green) and north-south component B_z (north, pink; south, red) in GSE coordinates. Also plotted are 3-hour estimated *Kp* index (red) and the 15-min predicted Costello *Kp* index (blue). (b) Cosmic ray density. (c) Cosmic ray intensity (circles) measured by a single Spaceship Earth station relative to the cosmic ray density. Red and blue circles indicate the deficit and excess intensity, respectively, and the radius of the circle scales with the magnitude of the deficit or excess; see right side of plot for scale. (d) Residual deviation after subtracting the fitted first-order anisotropy from each station. Red and blue circles represent deficit and excess relative to a first-order anisotropy. In Figures 5c and 5d, vertical axes indicate the pitch angle (see text).

where $I_{i,j}^{fit}$ is the intensity measured by the *j*th directional channel in the *i*th muon detector. This yields for each hour the best fit density of primary cosmic rays (i.e., the omnidirectional component of intensity) as well as the three components of the streaming vector, or first-order anisotropy, in the geographic (GEO) coordinate system (ξ_x^{GEO}, ξ_y^{GEO}, ξ_z^{GEO}). In equation (2), t_i is the local time in hours at the *i*th station; ω is $2\pi/24$h; and c_0^0, etc., are so-called "coupling coefficients." We then obtain the anisotropy vector in the GSE coordinate system (ξ_x, ξ_y, ξ_z) by a coordinate transformation.

[21] Figure 5 shows a sample loss cone display and bidirectional streaming display, together with IMF magnitude and B_z component, *Kp* index, and the cosmic ray density determined by fitting a first-order anisotropy for the period that a large Forbush decrease was observed. We display the 1-min ACE magnetic field data for the IMF and the estimated 3-hour and predicted (Costello) 15-min data for *Kp* index. These IMF and *Kp* indices are provided in real time at the Space Environment Center of NOAA (see http://www.sec.noaa.gov). In Figure 5c (loss cone display), we plot a pitch angle distribution of the intensity

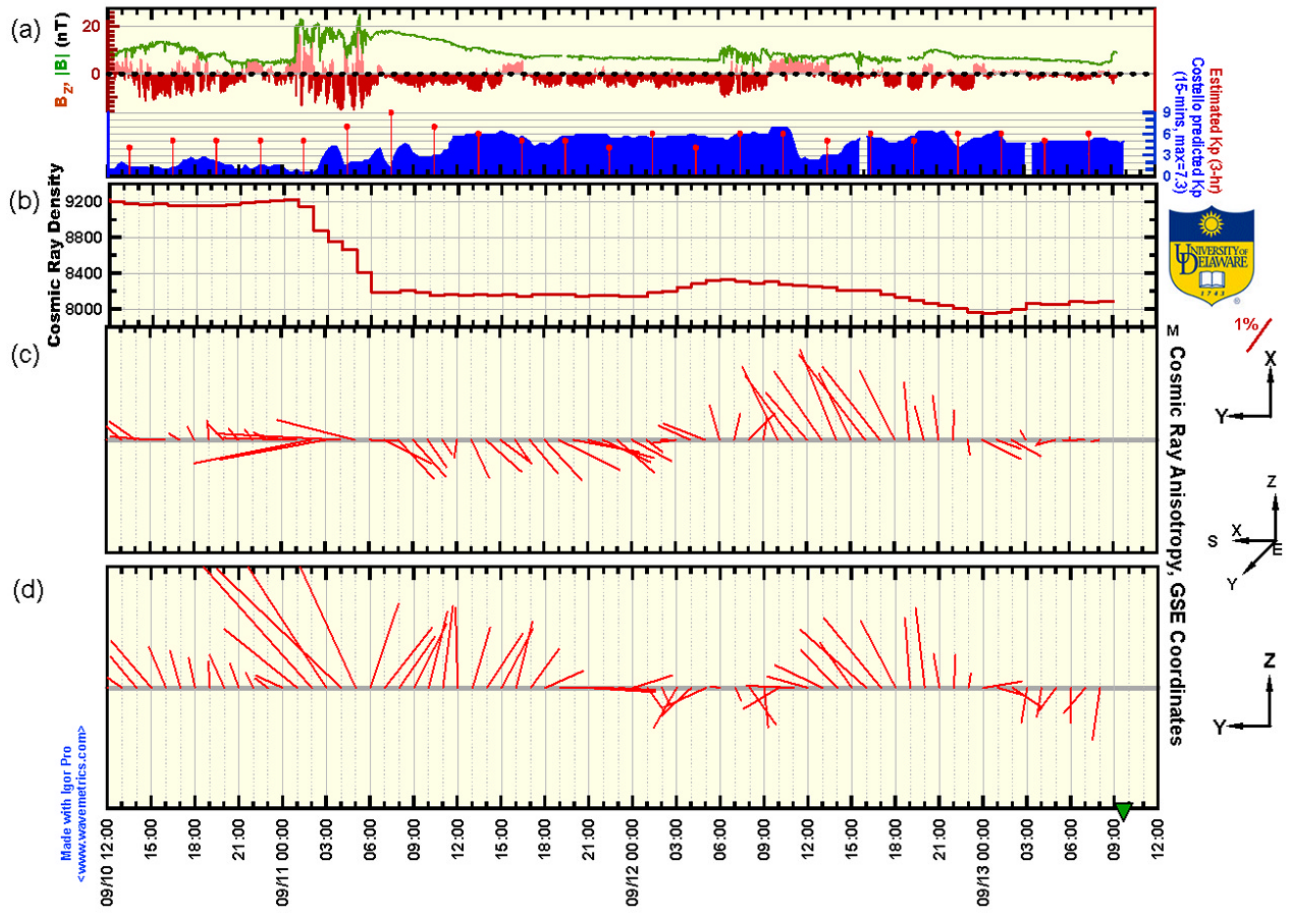

Figure 6. Sample cosmic ray flow direction in September 2005. (a) Plotted are 1-min ACE magnetic field magnitude $|B|$ (green) and north-south component B_z (pink-red) in GSE coordinates. Also plotted are 3-hour estimated *Kp* index (red) and the 15-min predicted Costello *Kp* index (blue). (b) Cosmic ray density. (c and d) Cosmic ray flow direction projected into the ecliptic plane and the plane oriented normal to the Sun-Earth line, as determined by fitting a first-order anisotropy to the network data. Flow direction is plotted in the GSE coordinate system (see text). Each red line segment represents an hourly measurement of the anisotropy, with the base plotted at the time of measurement and the head oriented according to the direction and magnitude of the anisotropy. We follow the meteorological convention; that is, arrows point in the direction that the flow is coming from.

variation from cosmic ray density. The pitch angle of each direction is the angle between the station-viewing direction of the median rigidity particle and the sunward magnetic field direction calculated as the hourly average of the ACE magnetic field data. Here "sunward" is defined relative to a nominal 45° spiral field; a station with zero degree pitch angle views particles coming from the Sun along the magnetic field. Each circle represents an hourly average of the cosmic ray intensity, and red and blue circles indicate the deficit and excess intensity, respectively. The defining characteristic of a loss cone precursor is a strong suppression of cosmic ray intensity for particles arriving from the sunward magnetic field direction. Thus large red circles, concentrated near small pitch angles, are indicative of a loss cone anisotropy. Shown in Figure 5d is the bidirectional streaming display. Each circle represents the residual deviation after subtracting the fitted first-order anisotropy from each station. The defining characteristic of a bidirectional flow is a strong elevation of cosmic ray intensity along the magnetic field (0° and 180° pitch angles) relative to the intensity at 90°. Thus blue circles concentrated near the edges of the plot, with red circles near 90°, are indicative of bidirectional cosmic ray streaming. In Figure 5, although a loss cone precursor was not observed (perhaps owing to poor coverage of the 0° pitch angle region before the arrival of the

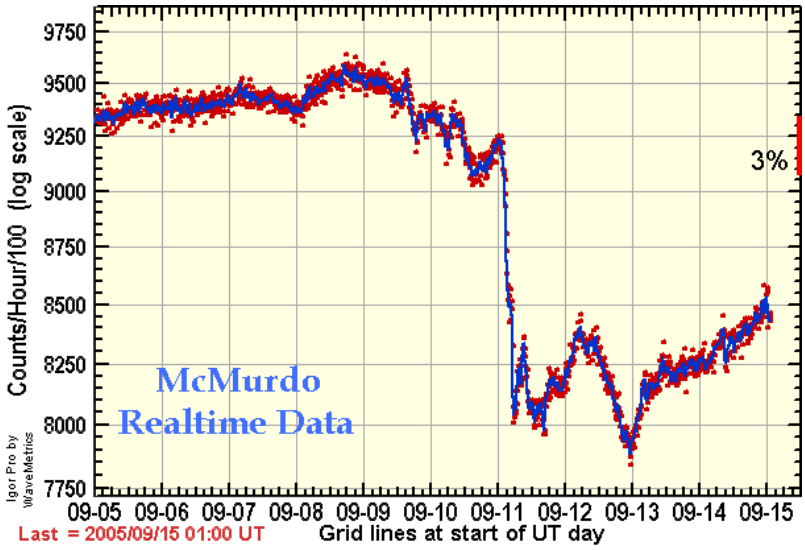

Figure 7. Individual station count rate measured in McMurdo, Antarctica. Last 10 days' pressure corrected count rate of McMurdo station are plotted. Each red point shows 10-min average value, and the blue line shows 1-hour centered moving average value.

shock and the resultant storm sudden commencement (SSC) at 0114 on 11 September), signs of bidirectional streaming were seen from 1800 on 11 September to 0300 on 12 September.

3.3. Cosmic Ray Flow Direction

[22] The first-order anisotropy determined by fitting network data specifies current conditions in the nearby interplanetary medium. It simply tells which way the (cosmic ray) "wind" blows and how strongly. Figure 6 shows a sample cosmic ray flow direction plot, together with IMF magnitude, *Kp* index, and the cosmic ray density determined by fitting a first-order anisotropy for the same period as Figure 5. Figures 6c and 6d show the anisotropy vector projected into the ecliptic plane (Figure 6c) and the plane normal to the Sun-Earth line. Flow direction is plotted in the GSE coordinate system; the x axis points toward the Sun (upward in Figure 6c), the y axis points opposite the direction of Earth's revolution about the Sun (leftward in Figures 6c and 6d), and the z axis points northward of the ecliptic plane (upward in Figure 6d). As shown in Figure 5, a strong variation of the anisotropy vector would typically be observed during the ICME passage and sometimes prior to shock arrival. This kind of anisotropy contains much information about the ICME. For example, three-dimensional cosmic ray density gradients are derived from this anisotropy vector and IMF vector and are available to deduce the ICME geometry in space [*Kuwabara et al.*, 2004].

3.4. Individual Station Count Rates

[23] Finally, we display individual station count rates. This simple plot tells us the time and scale of the Forbush decrease and GLE as observed at a single location on Earth's surface. For neutron monitor count rates, six stations (South Pole, McMurdo, Thule, Inuvik, Fort Smith, and Newark) operated by the University of Delaware are displayed. Figure 7 shows the counting rate of the McMurdo station. The last 10 days of data are plotted in real time. On the Web site, neutron monitor count rates are displayed over two time periods: the last 10 days and the last 6 months. All muon detector count rates are similarly displayed on the Web site, but only five selected directions are shown. Muon count rates are provided with periods of the last 3 days and the last 27 days.

4. Summary

[24] We have developed a real-time monitoring system of high-energy cosmic rays for space weather. Neutron monitors and muon detectors provide the data for our system and make it possible to observe cosmic rays with dual energy range observation. Moreover, these detectors are located all over the world and accurately detect the intensity variation and anisotropy in near-Earth space. The GLE monitor displaying 14 neutron monitor count rates provides a tool for early detection of SEP event onset. A loss cone display and bidirectional streaming display show the pitch angle distribution of the cosmic ray intensity variation. They can detect the precursor anisotropy prior to arrival of the ICME and particle bidirectional streaming inside the ICME. The cosmic ray flow direction plotting the first-order anisotropy shows the particle flow direction and its magnitude. Individual station count rates tell us the time and scale of the Forbush decrease and GLE event at a single location. These displays are made by real-time data processing and are updated to a World Wide Web server. It provides a new tool for space weather

forecasting and for specifying conditions in the near-Earth space environment. This tool will become even more useful and reliable in the future, as more stations of the worldwide neutron monitor and muon detector networks become available in real time.

[25] **Acknowledgments.** This work is supported in part by U.S. NSF grants ATM-0207196 and ATM-0527878 and in part by a Grants-in-Aid for Scientific Research from the Ministry of Education, Culture, Sports, Science and Technology in Japan and by the joint research program of the Solar-Terrestrial Environment Laboratory, Nagoya University. The authors gratefully acknowledge FAPESP (05/54800-1) for the scholarship to M. R. Silva.

References

Belov, A. V., L. I. Dorman, E. A. Eroshenko, N. Iucci, G. Villoresi, and V. G. Yanke (1995), Search for predictors of Forbush decreases, paper presented at 24th International Cosmic Ray Conference, Comm. on Cosmic Rays of the Int. Union of Pure and Appl. Phys., Comm. on Cosmic Rays of the Int. Union of Pure and Appl. Phys., Rome.

Belov, A. V., J. W. Bieber, E. A. Eroshenko, P. Evenson, R. Pyle, and V. G. Yanke (2001), Pitch-angle features in cosmic rays in advance of severe magnetic storms: Neutron monitor observations, paper presented at 27th International Cosmic Ray Conference, Comm. on Cosmic Rays of the Int. Union of Pure and Appl. Phys., Hamburg, Germany.

Bieber, J. W., and P. Evenson (1995), Spaceship Earth—An optimized network of neutron monitors, paper presented at 24th International Cosmic Ray Conference, Comm. on Cosmic Rays of the Int. Union of Pure and Appl. Phys., Rome.

Bieber, J. W., and P. Evenson (1998), CME geometry in relation to cosmic ray anisotropy, *Geophys. Res. Lett.*, *25*, 2955–2958.

Bieber, J. W., P. Evenson, R. Pyle, A. Belov, and E. Eroshenko (1999), Bidirectional flows of relativistic cosmic rays in solar ejecta, *Eos Trans. AGU*, *80*(46), Fall Meet. Suppl., Abstract SH42B-11.

Bieber, J. W., J. Clem, P. Evenson, R. Pyle, D. Ruffolo, and A. Saiz (2004), Spaceship Earth observations of the Easter 2001 solar particle event, *Astrophys. J.*, *601*, L103–L106.

Cane, H. V. (2000), Coronal mass ejections and Forbush decreases, *Space Sci. Rev.*, *93*, 55–77.

Clem, J. M., and L. I. Dorman (2000), Neutron monitor response functions, *Space Sci. Rev.*, *93*, 335–359.

Dvornikov, V. M., and V. E. Sdobnov (2002), Variations in the rigidity spectrum and anisotropy of cosmic rays at the period of Forbush effect on 12–25 July 1982, *Int. J. Geomagn. Aeron.*, *3*(3), 217–228.

Dvornikov, V. M., V. E. Sdobnov, and A. V. Sergeev (1983), Analysis of cosmic ray pitch-angle anisotropy during the Forbush-effect in June 1972 by the method of spectrographic global survey, paper presented at International Cosmic Ray Conference, Comm. on Cosmic Rays of the Int. Union of Pure and Appl. Phys., Bangalore, India.

Forbush, S. E. (1938), On world-wide changes in cosmic-ray intensity, *Phys. Rev.*, *54*, 975–988.

Fujimoto, K., A. Inoue, K. Murakami, and K. Nagashima (1984), Coupling coefficients of cosmic ray daily variations for meson telescopes, *Rep. 9*, Cosmic Ray Res. Lab., Nagoya, Japan.

Gosling, J. T., S. J. Bame, D. J. McComas, and J. L. Phillips (1990), Coronal mass ejections and large geomagnetic storms, *Geophys. Res. Lett.*, *17*, 901–904.

Kuwabara, T., et al. (2004), Geometry of an interplanetary CME on October 29, 2003 deduced from cosmic rays, *Geophys. Res. Lett.*, *31*, L19803, doi:10.1029/2004GL020803.

Leerungnavarat, K., D. Ruffolo, and J. W. Bieber (2003), Loss cone precursors to Forbush decreases and advance warning of space weather effects, *Astrophys. J.*, *593*, 587–596.

McDonald, F. B. (2000), Integration of neutron monitor data with spacecraft observations: A historical perspective, *Space Sci. Rev.*, *93*, 263–284.

Morishita, I., K. Nagashima, S. Sakakibara, and K. Munakata (1990), Long term changes of the rigidity spectrum of Forbush decrease, paper presented at 21st International Cosmic Ray Conference, Comm. on Cosmic Rays of the Int. Union of Pure and Appl. Phys., Adelaide, S. Aust., Australia.

Morishita, I., et al. (1997), Characteristics of precursory decrease of Forbush decrease inferred from world wide observations of muon and neutron intensities, paper presented at 25th International Cosmic Ray Conference, Comm. on Cosmic Rays of the Int. Union of Pure and Appl. Phys., Durban, South Africa.

Munakata, K., J. W. Bieber, S. Yasue, C. Kato, M. Koyama, S. Akahane, K. Fujimoto, Z. Fujii, J. E. Humble, and M. L. Duldig (2000), Precursors of geomagnetic storms observed by the muon detector network, *J. Geophys. Res.*, *105*, 27,457–27,468.

Munakata, K., et al. (2005), CME-geometry and cosmic-ray anisotropy observed by a prototype muon detector network, *Adv. Space Res.*, *36*, 2357–2362.

Nagashima, K., K. Fujimoto, and I. Morishita (1994), Interplanetary magnetic field collimated cosmic ray flow across magnetic shock from inside of Forbush decrease, observed as local-time-dependent precursory decrease on the ground, *J. Geophys. Res.*, *99*, 21,419–21,428.

Richardson, I. G., V. M. Dvornikov, V. E. Sdobnov, and H. V. Cane (2000), Bidirectional particle flows at cosmic ray and lower ($\sim$1 MeV) energies and their association with interplanetary coronal mass ejections/ejecta, *J. Geophys. Res.*, *105*, 12,579–12,592.

Ruffolo, D. (1999), Transport and acceleration of energetic particles near an oblique shock, *Astrophys. J.*, *515*, 787–800.

Simpson, J. A., W. Fonger, and S. B. Treiman (1953), Cosmic radiation intensity-time variations and their origin. I. Neutron intensity: Variation method and meteorological factors, *Phys. Rev.*, *90*, 934–950.

S. Akahane, C. Kato, M. Koyama, K. Munakata, and S. Yasue, Physics Department, Shinshu University, Matsumoto 390-8621, Japan. (sakahane@denshi.shinshu-u.ac.jp; ckato@corona.shinshu-u.ac.jp; mkoyama@shinshu-u.ac.jp; kmuna00@shinshu-u.ac.jp; shyasue@shinshu-u.ac.jp)

J. W. Bieber, J. Clem, P. Evenson, T. Kuwabara, and R. Pyle, Bartol Research Institute and Department of Physics and Astronomy, University of Delaware, Newark, DE 19716, USA. (john@bartol.udel.edu; clem@bartol.udel.edu; penguin@bartol.udel.edu; takao@bartol.udel.edu; pyle@bartol.udel.edu)

M. L. Duldig, Australian Antarctic Division, Kingston, Tas 7050, Australia. (marc.duldig@aad.gov.au)

Z. Fujii, Solar-Terrestrial Environment Laboratory, Nagoya University, Nagoya, Aichi 464-8601, Japan. (fujii@stelab.nagoya-u.ac.jp)

W. D. Gonzalez, M. R. Silva, N. J. Schuch, and N. B. Trivedi, Southern Regional Space Research Center, National Institute for Space Research, Santa Maria, RS 97105-900, Brazil. (gonzalez@dge.inpe.br; marlos@lacesm.ufsm.br; njschuch@lacesm.ufsm.br; trivedi@lacesm.ufsm.br)

J. E. Humble, School of Mathematics and Physics, University of Tasmania, Hobart, Tas 7001, Australia. (john.humble@utas.edu.au)